ACS Catalysis

Article

Dynamic behavior of Pd/P4VP catalyst during the aerobic oxidation of 2-propanol: a simultaneous SAXS/XAS/MS operando study

Elena Groppo, Andrea Lazzarini, Michele Carosso, Aram L. Bugaev, Maela Manzoli, Riccardo Pellegrini, Carlo Lamberti, Dipanjan Banerjee, and Alessandro Longo

ACS Catal., **Just Accepted Manuscript** • DOI: 10.1021/acscatal.8b01421 • Publication Date (Web): 13 Jun 2018

ACS Publications

is published by the American Chemical Society. 1155 Sixteenth Street N.W., Washington, DC 20036

Dynamic behavior of Pd/P4VP catalyst during the aerobic oxidation of 2-propanol: a simultaneous SAXS/XAS/MS *operando* study

Elena Groppo,[1,]* Andrea Lazzarini,[1,2] Michele Carosso,[1] Aram Bugaev,[3] Maela Manzoli,[4] Riccardo Pellegrini,[5] Carlo Lamberti,[3,6] Dipanjan Banerjee,[7] Alessandro Longo[8,]*

[1] Department of Chemistry, INSTM and NIS Centre, University of Torino, via Quarello 15, I-10135 Torino (Italy)
[2] Centre for Materials Science and Nanotechnology, Department of Chemistry, University of Oslo, Sem Saelands vei 26, N-0315 Oslo, Norway.
[3] The Smart Materials Research Center, Southern Federal University, Zorge Street 5, 344090 Rostov-on-Don, Russia.
[4] Department of Drug Science and Technology, NIS Centre and INSTM, University of Turin, Via Pietro Giuria 9, Turin, I-10125, Italy.
[5] Chimet SpA - Catalyst Division, Via di Pescaiola 74, Viciomaggio Arezzo, I-52041, Italy
[6] Department of Physics and CrisDi Interdepartmental Centre, University of Turin, via Pietro Giuria 1, 10125 Turin, Italy.
[7] Department of Chemistry, KU Leuven, Celestijnenlaan 200F box 2404, 3001 Leuven, Belgium
[8] Netherlands Organization for Scientific Research at ESRF, BP 220, F-38043 Grenoble Cedex 9, France

Abstract

The behaviour of a $Pd(OAc)_2$/P4VP catalyst submitted to different pre-treatments (pre-reduced, pre-oxidised and un-treated) during the aerobic oxidation of 2-propanol to acetone in the gas phase has been investigated. Synchronous, time-resolved, SAXS/XAS/MS techniques coupled with *operando* DRIFT spectroscopy (which gave information on the destiny of the acetate ligands) and ex-situ HR-TEM (to detect the formation of Pd nano-particles and to obtain their size distribution) were employed to accomplish a dynamical picture of the changes occurring to the Pd phase under transient reaction conditions. In addition, the catalytic performances were qualitatively explored by means of a CATLAB micro-reactor, with the final aim to establish structure-activity relationships. Our approach clearly demonstrates that highly isolated Pd^{2+} cationic species, either atomically dispersed or in the form of ultra-small Pd^{2+}-oxo clusters, are efficient and very stable active sites for the gas-phase aerobic oxidation of 2-propanol to acetone. Noticeably, the behaviour of the $Pd(OAc)_2$/P4VP catalyst in reaction conditions are influenced by the nature of the support. On one hand, the presence of the pyridyl functional groups is fundamental to stabilize the cationic Pd^{2+} species, on the other hand, the porous structure of the P4VP polymer efficiently confine the active Pd^{2+} species in the presence of the reagents. As such, our catalyst is situated at the confluence between its homogeneous and heterogeneous analogues.

Keywords: alcohol oxidation, palladium, SAXS, XAS, operando

1. Introduction

Selective aerobic oxidation of alcohols to their corresponding aldehydes over noble-metal-based catalysts is an environmentally benign process in fine chemistry, but also a reaction particularly demanding, because it requires the activation of molecular oxygen and C-O bonds in close proximity, at temperatures typically below 160 °C.[1-5] The economic and environmental advantages of molecular oxygen as a chemical oxidant are readily apparent: oxygen is abundant, inexpensive and thermodynamically potent. However, effective solutions to this problem must overcome the intrinsic reactivity and selectivity challenges posed by the chemistry of O_2: O_2 is a four-electron oxidant when it is reduced to water but most desired reactions are 2-electron oxidations, and partially reduced oxygen species are typically more reactive and potent oxidants than O_2 itself.[6-9] Both heterogeneous and homogeneous Pd-based catalysts are largely employed in selective alcohol oxidations, on account of the Pd ability to perform selective oxidations at temperatures typically between 60 and 160 °C and atmospheric oxygen pressure.[1-6] Albeit significant progresses have been achieved in understanding the role of Pd-based catalysts by using *in situ* or *operando* spectroscopic[10-12] and microscopic[13,14] tools, the mechanism of the reaction is still a matter of discussion.[15-17]

It has long being accepted that the reaction proceeds following an oxidase-style mechanism consisting of two steps: 1) a Pd-mediated oxidation of the alcohol by dehydrogenation, with the formation of the corresponding aldehyde and of a Pd-hydride intermediate; and 2) the aerobic oxidation of the reduced catalyst. The two stages occur independently and in sequence.[1-6,18,19] According to this mechanism molecular oxygen is not directly involved in the substrate oxidation, but has the double role of re-oxidizing the Pd-hydrides (supported by the observation that O_2 can be replaced by an hydrogen-acceptor),[20,21] and suppressing the decarbonylation of the oxidation products over metallic Pd. [1-5] Competing reactions may occur at specific surface sites[19] during the catalytic cycles (such as the decarbonylation or the over-oxidation of the products, over-oxidation of the catalyst, aggregation of Pd species to inactive bulk metal), with a consequent decrease in selectivity and de-activation of the catalyst.

In both homogeneous and heterogeneous cases, the unambiguous identification of the oxidation state (Pd(II) or Pd(0)) and of the aggregation of the Pd species during the catalysis has a pivotal importance. The aerobic oxidation of alcohols was investigated both in liquid phase (aqueous media or organic solvents)[16,22-25] and in the gas phase,[26,27] by X-ray absorption spectroscopy (XAS) coupled with vibrational spectroscopies and/or electrochemical measurements. For Pd-based heterogeneous catalysts, it was early discovered that the rate of alcohol oxidation is higher on a reduced metal surface than on an oxidized one.[1,28,29] Several works indicate that metallic Pd is the catalytically active phase. Interestingly, in most of these studies it was also reported that the introduction of oxygen in the reactant feed causes a sudden increase of the alcohol conversion, observation that was attributed to a cleaning of the Pd surface by oxygen, rather than to a change in the Pd oxidation state. Other studies[30-35] indicate that surface PdO is the active phase in alcohol oxidation reactions, and that the oxide-to-metal structural transition is accompanied by catalyst deactivation through secondary decarbonylation of the products.

The nature of the active Pd sites during alcohol oxidation is similarly uncertain also for homogeneous Pd-based catalysts.[6,36-41] For the $Pd(OAc)_2$/pyridine system, Steinhoff et al. detected (by means of *in situ* spectroscopy) a Pd(II) resting state.[17,42,43] However, Uemura et al.,[44] proposed an alternative hypothesis, wherein Pd remains in the +2 oxidation state throughout the catalytic cycle. The above mentioned $Pd(OAc)_2$/pyridine homogeneous system is one of the most efficient and selective catalyst for oxidation of alcohols to aldehydes.[17,36,42-46] All the major classes of alcohols (primary, secondary, benzylic, and allylic) are oxidized in toluene solution at 80 °C, generally in good-to-excellent yields (80–100%).[36] In this system the labile pyridine ligands greatly facilitate the reductive elimination of the aldehyde from the Pd-H intermediate and therefore significantly enhance the rate of Pd(0) oxidation by molecular oxygen. When the efficiency of this second step diminishes (i.e. in absence or in defect of oxygen) the catalyst is deactivated through the formation of Pd nanoparticles.

Recently, we have been involved in the study of the chemistry of $Pd(OAc)_2$ inside a porous, divinylbenzene cross-linked, pyridine-containing polymer (P4VP).[47-50] In the freshly prepared form this system might be seen as the heterogeneous counter-part of $Pd(OAc)_2$/pyridine, and this stimulated us to explore its behaviour during the aerobic oxidation of an alcohol in the gas phase, as a function of the reaction conditions. In particular, we applied synchronous, time-resolved, SAXS/XAS/MS techniques to obtain a dynamical picture of the changes occurring to the Pd species (in terms of oxidation state, aggregation, and local structure) under transient reaction conditions. The SAXS/XAS/MS measurements were complemented with two additional characterization techniques: 1) *operando* DRIFT spectroscopy, to interrogate the destiny of the acetate ligands; 2) *ex-situ* HR-TEM, to directly visualize the eventual presence of Pd nanoparticles and to evaluate their particle size distribution. Finally, the catalytic performances were qualitatively explored by means of a CATLAB micro-reactor, with the final aim to correlate the catalyst properties to the catalytic performances. We selected 2-propanol as reactant, because of its high vapour pressure that allows performing the experiments in the gas-phase, thus avoiding competitive solvent effects. In addition, it is easy to handle, non-toxic, with a low boiling point and a flash point at higher temperatures with respect to other alcohols. Finally, 2-propanol is the simplest secondary alcohol, and it can be oxidized solely to acetone, thus simplifying the catalytic study. Although oxidation of 2-propanol to acetone is not relevant from a technological point of view (acetone is produced directly or indirectly from propylene, mainly via the cumene process), our spectroscopic results indicate the occurrence of a single site mechanism for the alcohol oxidation reaction that might be of potential help in developing more performant catalysts for selective alcohol oxidation.

2. Experimental

2.1 Catalyst preparation

The $Pd(OAc)_2$/P4VP catalyst was prepared in the Chimet laboratories starting from Pd(II) acetate (hereafter $Pd(OAc)_2$) and a poly-4-vinyl-pyridine 25% crosslinked with divinylbenzene (Sigma Aldrich, hereafter P4VP), showing a specific surface area of about 50 m^2g^{-1}. P4VP (in the form of micro-spheres) was added to an orange solution of

$Pd(OAc)_2$ in acetonitrile containing 4 wt% of Pd[51] with respect to the support and left under stirring at room temperature overnight.[47,48] The solution appeared completely decoloured, the sample was filtered, successively dried at room temperature and mildly ground in an agate mortar when necessary. We demonstrated previously[48] that the $Pd(OAc)_2$ precursor is stabilized inside the P4VP scaffold through the coordination of the pyridyl groups to the Pd^{2+} cations, with the consequent rupture of the trimeric structure characteristic for solid $Pd(OAc)_2$, and the restructuring of the acetate ligands in a mono-dentate coordination.

2.2 Treatment protocols

Before investigating the catalyst changes during the aerobic oxidation of 2-propanol, the effect of the two reagents alone was explored. Reduction in 2-propanol was accomplished by feeding in the reactor (either the capillary in SAXS/XAS/MS measurements or the DRIFTS cell for the FT-IR measurements) the vapours of the alcohol stripped by an inert flow (He, 20 ml/min) at 50 °C, and increasing the temperature up to 200 °C (ramp 2 °C/min). Oxidation of the catalyst was achieved by flowing in the reactor a 15% O_2 in He flow (20 ml/min of total flow) at 50 °C and successively increasing the temperature up to 200 °C (ramp 2 °C/min). The aerobic oxidation of 2-propanol was conducted on the catalysts 1) pre-reduced in 2-propanol, 2) pre-oxidized in O_2, and 3) fresh. The reaction was performed by feeding in the reactor the vapours of the alcohol stripped by a 15% O_2/He flow at 50 °C, and successively increasing the temperature up to 180 °C. The temperature was limited to 180 °C owing to the observation that at higher temperature the complete combustion of 2-propanol was favoured.

2.3 Characterization techniques and data analysis

2.3.1 Synchronous SAXS/XAS/MS measurements

Synchronous SAXS/XAS/MS measurements were performed on the BM26A beamline at the ESRF facility (Grenoble, France), by using the experimental set-up reported previously.[48,52,53] The catalyst powder was placed in a 2 mm glass capillary, having upstream and downstream two small pieces of quartz wool. The capillary was connected to the BM26A gas rig for with mass-flow controllers for gas delivery,[54] and heated with a heat gun. The evolution of the gaseous products of reaction are monitored with an online mass spectrometer (MS) at the end of the capillary by sampling a fraction of the out-stream flow.

Transmission XAS spectra at the Pd K edge (24350 eV) were collected using an ionization chamber before the sample and an X-ray sensitive photodiode placed in the centre of the SAXS detector. The white beam was monochromatized using a Si(111) double crystal and harmonic rejection was performed by using Pt coated mirrors (horizontal acceptance 2 mrad). The beam was focused in order to achieve 1.5 x 1 mm dimension on the sample. The energy was calibrated measuring the XANES spectrum of a palladium foil. The XAS spectra were acquired in the 24200 – 24600 eV range with an energy step of 3 eV and an integration time of 1 s/point in the pre-edge region, 1.5 eV step and 3 s/point in the XANES region, while the step in the EXAFS region was chosen to obtain a 0.05 $Å^{-1}$ step in the *k*-space with the acquisition time increasing quadratically from 3 to 9 s/point. Each spectrum required an acquisition time of about 10 minutes as compromise between fast acquisition and quality of the spectra. It is worth noticing that, according to literature,[18,27] the reaction induced restructuring of Pd nanoparticles equilibrates within ca. 10 seconds during the vapour phase selective oxidation of crotyl alcohol. Hence, the timescale for spectra acquisition is long enough to allow our system equilibrating at each temperature. The spectra were normalized and analysed in the frame of multiple scattering theory with the GNXAS package software.[55,56] The details of the data analysis are reported in Section S2.

Simultaneously with XAS, SAXS patterns were collected by using a 2D Mar CCD detector. The sample-detector distance was calibrated accordingly to the peak position of a standard Ag behenate powder sample. The energy change between the start and the end of the XAS spectrum (about 80 eV) is irrelevant to SAXS so that the incident beam wavelength can be treated as constant, λ=0.509(1) Å. At this energy, we cover a q range ($q = 4\pi \sin\theta/\lambda$; 0.01-0.3 $Å^{-1}$) big enough to get information on the size and the shape of eventually formed nanoparticles. A SAXS pattern was collected for each XAS spectrum. The patterns were integrated with Fit2D[57] and modelled with a home-made code.[53,58]

The SAXS data have been analysed by fitting the experimental patterns with the function described by Eq. (1):

$$I(q)=A+\frac{B}{q^4}+C\int D(r)j(qR)^2r^6dr \qquad \text{Eq. (1)}$$

where the term $A+B/q^4$ describes the Porod function,[59] simulating the polymer contribution; D(r) corresponds to the Weibull function, accounting for the particle size distribution, which is in turn defined as $D(r) = (r/R)^{-1}\exp(-r/R)^b$, in which R is the average radius of the particles and j(qR) is the spherical first order Bessel function, accounting for the spherical shape of the metal clusters.

2.3.2 DRIFT spectroscopy

FT-IR spectra were collected in diffuse reflectance mode (DRIFT) on a Nicolet 6700 instrument, equipped with a MCT detector. A Thermo-Fisher Environmental Chamber was used to record the FT-IR spectra under reaction conditions. The cell was connected to a gas-flow system (under atmospheric pressure), equipped with electronic mass flow controllers (MFC). Each FT-IR spectrum required an acquisition time of about 2 minutes. FT-IR spectra were recorded at regular time interval, during the whole process at a spectral resolution of 4 cm^{-1}. Just at the end of each experiment, the catalyst powder was recovered and immediately measured by HR-TEM, trying to minimize the exposure to air.

2.3.3 High resolution Transmission Electron Microscopy

High Resolution Transmission electron micrographs (HR-TEM) were obtained using a JEOL 3010-UHR instrument operating at 300 kV, equipped with a LaB_6 filament and fitted with X-ray EDS analysis by a Link ISIS 200 detector. Digital micrographs were acquired by a 2k × 2k pixel Gatan US1000 CCD camera. Samples were quickly deposited (in the dry form, i.e. without using any solvent) on a copper grid covered with a lacey carbon film. Histograms of the particle size distribution were obtained by considering a statistical representative number of particles on the HR-TEM images, and the mean particle diameter (d_{TEM}) was calculated as:

$$\langle d_{TEM}\rangle=\frac{\sum d_i n_i}{\sum n_i} \qquad \text{Eq. (2)}$$

where n_i was the number of particles of diameter d_i.

2.4 Catalytic tests

For the catalytic tests, an integrated quartz micro-reactor and mass spectrometer system (CATLAB from Hiden) was adopted. The system features a fast-response, low thermal mass furnace with integrated air-cooling, a precision quadrupole mass spectrometer, and a quartz inert capillary with "hot zone" inlet for continuous close-coupled catalyst sampling with minimal dead volume and memory effects. The catalyst was loaded into the quartz reactor with an inner diameter of 10 mm. The reaction temperature was monitored by using an in-bed thermocouple that ensures optimal measurement of catalyst temperature. The reactant gases were fed through electronic mass flow controllers. Feed and product analysis were performed by using a Pfeiffer OmniStar quadrupole Mass Spectrometer, monitoring the following ionic masses: (*m/Z*) = 4 (He), 18 (H_2O), 28 (CO_2), 32 (O_2), 43 (acetone), 45 (2-propanol), 60 (acetic acid). It is worth noticing that 2-propanol contributes also to the intensity of mass 43, that however is the most intense fragment for acetone.

3. Results and Discussion

3.1 $Pd(OAc)_2$/P4VP reduced in 2-propanol and its catalytic performances

3.1.1 Reactivity of $Pd(OAc)_2$/P4VP with 2-propanol

The ability of simple alcohols in reducing palladium oxide in mild conditions has been known since long time.[1] Newton et al.[60] have recently proved that also ethanol-water, a prototypical "green" solvent mixture, cannot be considered as innocent toward supported Pd nanoparticles. Even dehydrogenation of the simplest secondary alcohol, 2-propanol, leads to PdO reduction and may poison metallic Pd already at room temperature.[1] Reduction of $Pd(OAc)_2$ is less easy than reduction of PdO: it does not occur at room temperature, but requires reaching ca. 110 °C and it is completed around 180 °C. In our previous work[50] we followed the reduction of $Pd(OAc)_2$ in 2-propanol by means of DRIFT spectroscopy, by monitoring the disappearance of the IR bands characteristic of the acetate ligands and by characterizing the obtained Pd nanoparticles by using CO as a probe molecule. The sequence of DRIFT spectra collected during the reaction are shown Figure S1 in the Supporting Information and here represented in a 2D map as a function of the temperature in Figure 1a, in the 1800 – 1250 cm^{-1} region. The two absorption bands at ca. 1365 and 1300 cm^{-1}, assigned to the ν_{sym}(COO) mode of two slightly different terminal acetate ligands (dotted lines in Figure 1a labelled as $Pd(OAc)_2$),[48] gradually decrease in intensity and are no more observed around 170 °C. Concomitantly, a shrinkage of the very intense band centred at 1596 cm^{-1} (assigned to the 8a vibrational mode of the pyridyl functional group) is observed (dotted line in Figure 1a labelled as py···Pd^{2+}), due to the disappearance of the shoulder at ca. 1640 cm^{-1}. This shoulder was previously considered as the fingerprint of a chemical interaction between the pyridyl groups of P4VP and the Pd^{2+} cations of the hosted $Pd(OAc)_2$,[48] similar to what was reported for several P4VP/metal complexes. [61-66]

At the end of the DRIFTS experiment, the sample was analysed by HR-TEM. A representative image is shown in Figure 1b, along with the particle size distribution determined by counting about 800 particles. Very small Pd nanoparticles, homogeneously distributed in the polymer, and with a spherical shape and a regular size are observed. Most of them have a diameter smaller than 2 nm and are hardly detectable by our TEM instrument. The average particle size ($\langle d_{TEM} \rangle$ = 1.4 ± 0.3 nm) is very similar to that of Pd particles obtained upon reducing the same system in H_2,[47,48] and reflects the stabilization effect of the pyridyl ligands in P4VP.

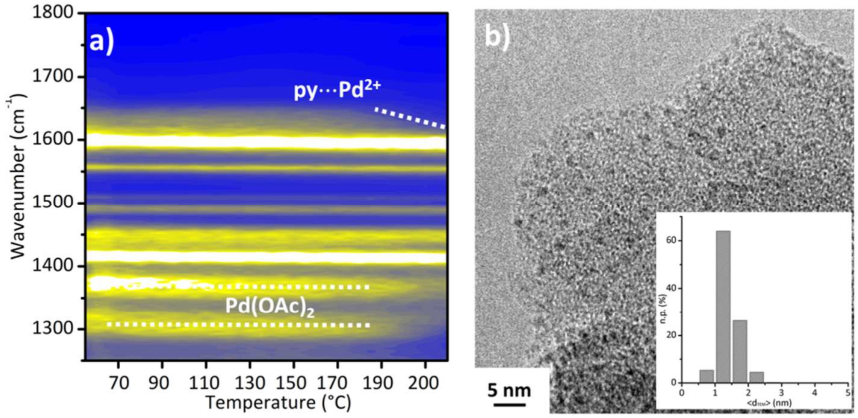

Figure 1. Part a): 2D map showing the evolution of the DRIFT spectra as a function of the reaction temperature, for the $Pd(OAc)_2$/P4VP reacting with 2-propanol. The intensity increases from blue to white. Dotted lines highlight the evolution of the absorption bands assigned to $Pd(OAc)_2$ and to the pyridyl groups of P4VP interacting with the hosted Pd^{2+} cations, respectively. Part b): Representative HR-TEM image of $Pd(OAc)_2$/P4VP after reaction with 2-propanol at 200 °C and corresponding particle size distribution.

To get insights into the mechanism of $Pd(OAc)_2$/P4VP reduction, the reaction of the catalyst with 2-propanol was followed by means of simultaneous, time–resolved, SAXS/XAS/MS measurements. Figure S2 in the Supporting Information shows the sequence of normalized XANES spectra, SAXS patterns and EXAFS spectra at the Pd K-edge collected simultaneously during the reaction of the $Pd(OAc)_2$/P4VP catalyst with 2-propanol upon increasing the temperature from 50 °C to 200 °C. A gradual change is observed by all three techniques starting from ca. 110 °C, while they did not evolve anymore once the temperature reached ca. 180 °C. This evolution indicates that the Pd^{2+} precursor is progressively reduced with the consequent formation of Pd^0 nanoparticles. The temperature interval during which $Pd(OAc)_2$ is reduced to Pd^0 nanoparticles is in very good agreement with that previously determined by DRIFT spectroscopy (Figure 1a). To better visualize the spectral changes as a function of the reaction temperature, the same data have been reported in 2D maps in Figure 2a-c, together with the evolution of the gaseous products of the reaction as simultaneously monitored by online MS (part d), and in the independent experiment with the CATLAB micro-reactor (part d'). Starting from the XANES spectra (Figure 2a), the following changes are observed during the reaction: 1) the edge (border between red and black regions) progressively shifts to lower energy; 2) the peak at ca. 24372 eV (labelled as Pd^{2+}), characteristic of $Pd(OAc)_2$, vanishes, and 3) is replaced by a peak at ca. 24386 eV (labelled as Pd^0), which is assigned to the first EXAFS oscillation of palladium atoms arranged in a face centred cubic (*fcc*) local structure, typical of Pd^0 nanoparticles.[47,48,67] Figure 2b shows the contribution of the spherical particles (either $Pd(OAc)_2$ or Pd^0, or both) with respect to the modelled background as determined by the analysis of the SAXS data. A gradual increase of the average particle size ($\langle d_{SAXS} \rangle$) is observed throughout the reaction, from ca. $\langle d_{SAXS} \rangle$ = 1.27 ± 0.05 nm to ca. 1.79 ± 0.05 nm, in good agreement with that determined by means of HR-TEM at the end of the reaction.

As far as the EXAFS spectra are concerned (Figure 2c), the peak initially at ca. 1.45 Å (not-phase corrected, labelled as Pd-O_{Ac}), attributed to the first shell Pd-O contribution of

$Pd(OAc)_2$, decreases in intensity and shifts at slightly higher distances (ca. 1.52 Å), while at the same time a new peak appears at ca. 2.55 Å (labelled as Pd-Pd), which is due to the first-shell Pd-Pd contribution of the Pd nanoparticles. The persistence of a signal around ca. 1.52 Å reveals that a substantial fraction of the Pd atoms interacts with low-Z elements. Since all the $Pd(OAc)_2$ has been reduced, this peak is attributed to the interaction of Pd either with the nitrogen of the pyridine ligands in P4VP[47,48] or with the carbon of carbonaceous species derived from the dehydrogenation of 2-propanol. Hereafter, we will refer to this peak as Pd-X contribution, where X states either for O, N or C (which are not distinguishable by EXAFS). The results of the EXAFS fits for each spectrum of the series are reported in Table S1 in the Supporting Information. Starting from ca. 130 °C the fraction of the Pd atoms in interaction with other Pd atoms (%Pd-Pd in Table S1) gradually increases, up to ca. 84% at the end of the reaction. In these conditions all the $Pd(OAc)_2$ has been reduced to Pd nanoparticles. The average coordination number $N_{Pd\text{-}Pd} = 2.6 \pm 0.5$ is extremely small compared with $N_{Pd\text{-}Pd} = 12$ in bulk Pd metal, as expected for very small nanoparticles.[68-73] Notably the results agree with literature data on similar systems[74-76] (more details are reported in the SI file).

In summary, $Pd(OAc)_2$ in P4VP is reduced by 2-propanol at elevated temperature to Pd^0 nanoparticles which are stabilized by the pyridyl moieties in P4VP. As far as the reduction mechanism is concerned, synchronous MS measurements detect small traces of acetic acid (*m/Z* = 60) during the reduction of $Pd(OAc)_2$ by 2-propanol (Figure 2d). This is confirmed by an independent catalytic test performed with the CATLAB micro-reactor (Figure 2d'). Acetic acid originates from the hydrogenation of the acetate ligands, and indicates the occurrence of alcohol dehydrogenation.

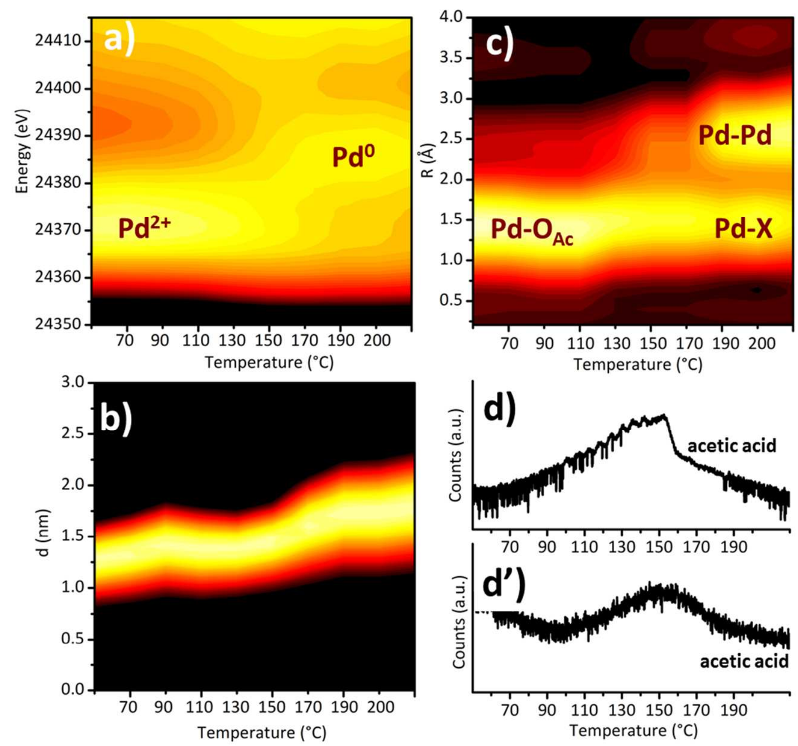

Figure 2. 2D maps showing the evolution of the XANES spectra (part a), of the particle size distribution as determined by the analysis of the SAXS data (part b), and amplitude of the phase-uncorrected FT of the EXAFS spectra (part c) as a function of the reaction temperature, for the $Pd(OAc)_2$/P4VP reacting with 2-propanol. The intensity increases from black to yellow. The labels refer to the main assignments. Parts d and

d' show the evolution of gaseous acetic acid (m/Z = 60) as detected by online MS and by the independent catalytic test performed with the CATLAB micro-reactor.

3.1.2 Catalytic performances of the $Pd(OAc)_2$/P4VP pre-reduced in 2-propanol

The $Pd(OAc)_2$/P4VP catalyst pre-reduced in 2-propanol efficiently catalyses the oxidation of 2-propanol to acetone. The reaction was initially followed by means of DRIFT spectroscopy. Figure S3 reports the evolution of the DRIFT spectra as a function of temperature, whereas Figure 3a shows the corresponding 2D map in the 1800 – 1680 cm^{-1} region, that is the region where acetone can be easily detected, because the characteristic ν(C=O) absorption band at ca. 1730 cm^{-1} does not overlap neither with those of the catalyst nor with those of 2-propanol. Acetone starts to be spectroscopically detected already around 80-90 °C, but the maximum conversion is achieved only at ca. 170-180 °C, in well agreement with the MS data (vide infra, Figure 4d and d'). After the reaction, the catalyst was also analysed by HR-TEM. A representative image and the particle size distribution are reported in Figure 3b. Despite the majority of the Pd NPs have preserved the initial small size, some very big Pd agglomerates, whose composition was checked by EDS analysis, have been observed (inset). With respect to the same catalyst before the aerobic oxidation of 2-propanol, a slight increase of the average particle size is detected ($\langle d_{TEM} \rangle$ = 1.6 ± 0.4 nm).

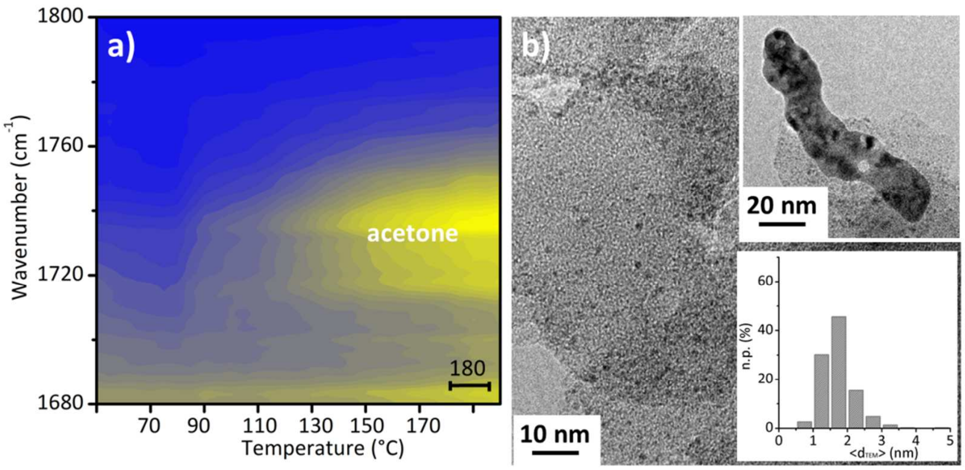

Figure 3. Part a): 2D map showing the evolution of the DRIFT spectra as a function of the reaction temperature, for the $Pd(OAc)_2$/P4VP catalyst pre-reduced in 2-propanol during the aerobic oxidation of 2-propanol to acetone. The intensity increases from blue to yellow. Part b): Two representative HR-TEM images of pre-reduced $Pd(OAc)_2$/P4VP after the aerobic oxidation of 2-propanol at 180 °C and corresponding particle size distribution.

The main question, however, is whether the catalyst works in the oxidized or in the reduced state. This is readily apparent by looking to Figure 4a-c, that shows the evolution of the XANES spectra (part a), of the particle size distribution as determined by the analysis of the SAXS data (part b), and of the amplitude of Fourier-transforms of (FT) of the EXAFS spectra (part c) during the oxidation of 2-propanol over the pre-reduced $Pd(OAc)_2$/P4VP catalyst as a function of the reaction temperature. The raw spectra are reported in Figure S4. As soon as the reaction starts (around 80-90 °C), the contributions due to metal Pd (i.e. the Pd^0 peak at ca. 24386 eV in the XANES spectra and the Pd-Pd contribution at ca. 2.55 Å in the EXAFS spectra) rapidly decrease in intensity and reach the minimum values around 110 °C. At the same time, the contributions ascribed to Pd^{2+} (the Pd^{2+} peak at ca. 24372 eV in the XANES spectra and the Pd-X contribution around 1.52 Å in the EXAFS spectra) increase in intensity, reaching the maximum values at ca. 160 °C. The fraction of the Pd atoms in interaction with other Pd atoms (%Pd-Pd in Table S2), as determined by fitting the EXAFS data, drastically decreases to less than 15%. The whole set of data clearly indicates that in the presence of the reaction mixture the Pd^0 nanoparticles are rapidly oxidized to PdO nanoparticles. The oxidation is almost complete because of their very small size. In the whole 110 – 170 °C interval, that corresponds to the best performance of the catalyst (Figure 4d and d'), the average oxidation state of palladium remains 2+, while the particle size changes are negligible ($\langle d_{SAXS} \rangle$ increases from 1.89 ± 0.05 nm to 1.96 ± 0.05nm, Figure 4c).

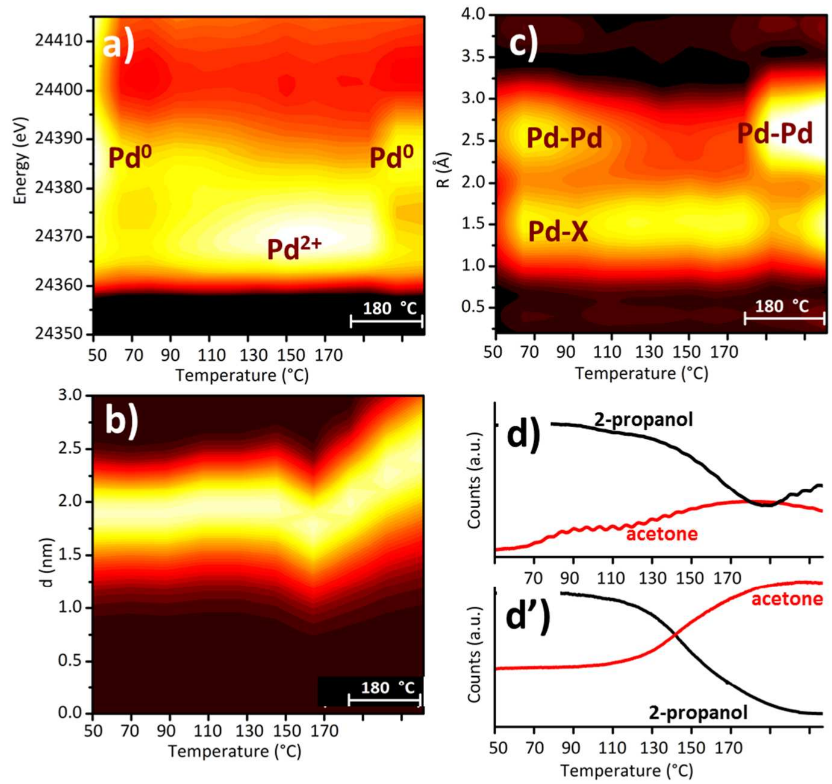

Figure 4. 2D maps showing the evolution of the XANES spectra (part a), of the particle size distribution as determined by the analysis of the SAXS data (part b), and of the amplitude of phase-uncorrected FT of the EXAFS spectra (part c) as a function of the reaction temperature, for the $Pd(OAc)_2$/P4VP pre-reduced in 2-propanol during the aerobic oxidation of 2-propanol. The intensity increases from black to yellow. The labels refer to the main assignments. Parts d and d' show the conversion of 2-propanol (m/Z = 45) into acetone (m/Z = 43) as detected by online MS and by an independent catalytic test performed with the CATLAB micro-reactor, respectively.

Around 170 – 180 °C a very sudden change is observed in all the spectra. The PdO nanoparticles are reduced back to Pd^0 and at the same time the particle size abruptly increases ($\langle d_{SAXS} \rangle$ goes from 1.96 ± 0.05nm to 2.45 ± 0.05 nm, Figure 4c)[77] and the %Pd-Pd (Table S1) reaches again a value of about 70%. The phenomenon is associated with a slight loss of the catalytic activity (Figure 4d and d'). The whole sequence of data presented so far converges in indicating that: 1) the pre-reduced $Pd(OAc)_2$/P4VP catalyst is rapidly oxidized in the presence of the reaction mixture and remains oxidized during the conversion of 2-propanol to acetone in the whole 110 – 170 °C temperature range, in agreement with recent studies that have implicated surface PdO as the active phase in the selective oxidation of alcohols;[30-35] 2) the pre-reduced $Pd(OAc)_2$/P4VP catalyst is not stable during the aerobic oxidation of 2-propanol at 170-180 °C. The reason for the instability of the Pd phase in these reaction conditions is not completely clear, but it might be associated with a sudden increase of the temperature at the catalyst surface. It is interesting to notice that the catalyst deactivation is not irreversible. Once that the catalyst is re-oxidized at 180 °C the activity is almost completely restored (data not shown), in a similar way to what reported in the literature for supported PdO_x nanoparticles.[26]

3.2 $Pd(OAc)_2$/P4VP oxidized in molecular O_2 and its catalytic performances

3.2.1 Reactivity of $Pd(OAc)_2$/P4VP with oxygen

Successively, we explored the reactivity of $Pd(OAc)_2$ towards molecular oxygen, which is the second reagent in the investigated reaction. Figure 5a shows the evolution of the DRIFT spectra for $Pd(OAc)_2$/P4VP in the presence of oxygen at increasing temperature from 50 °C to 200 °C (the corresponding spectra are reported in Figure S5). The two absorption bands at ca. 1365 and 1300 cm^{-1} characteristic of the acetate ligands[48] start to decrease in intensity when the temperature approaches 180 °C, although they do not completely disappear even at 200 °C. This indicates that a fraction of the acetate ligands is removed. At the same time, the shoulder at ca. 1640 cm^{-1}, indicative of the chemical interaction between the pyridyl groups of P4VP and the Pd^{2+} cations of $Pd(OAc)_2$ does not disappear (as observed for the reaction of $Pd(OAc)_2$/P4VP with 2-propanol), but further shifts to ca. 1665 cm^{-1} (dotted line in Figure 5a). A larger up-ward shift of the 8a vibrational mode of the pyridyl moieties indicates that these functional groups in P4VP interact with stronger acid sites, as it might be the case for Pd^{2+} cations that have lost one or both the acetate ligands. Interestingly, almost no nanoparticles were detected by means of HR-TEM at the end of the oxidation reaction (Figure 5b), signifying either that the acetate ligands are burnt off leaving isolated Pd^{2+} cations stabilized by the P4VP environment, or that extremely dispersed PdO clusters, with size below the detection limit of our TEM instrument, are formed.

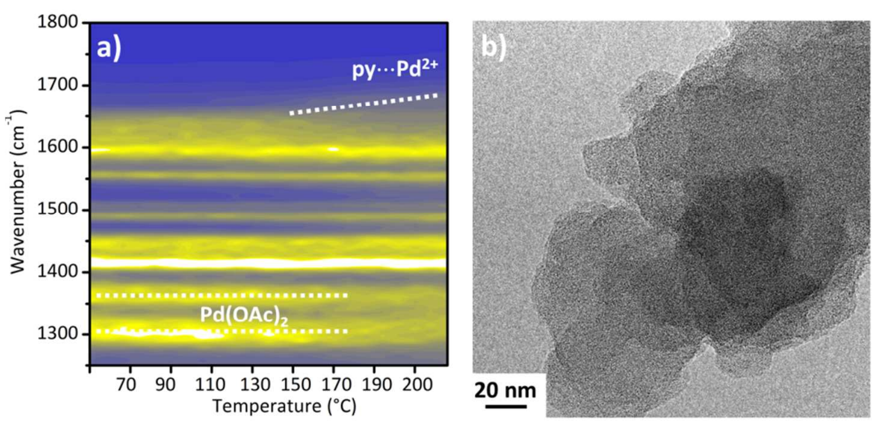

Figure 5. Part a): 2D map showing the evolution of the DRIFT spectra as a function of the reaction temperature, for the $Pd(OAc)_2$/P4VP catalyst during the reaction with molecular oxygen. The intensity increases from black to yellow. Dotted lines highlight the evolution of the absorption bands assigned to

$Pd(OAc)_2$ and to the pyridyl groups of P4VP in interaction with $Pd(OAc)_2$, respectively. Part b): A representative HR-TEM image of $Pd(OAc)_2$/P4VP after the reaction with molecular oxygen at 180 °C.

The results of the synchronous XAS/SAXS/MS experiment in the presence of molecular oxygen are reported in Figure 6, while the raw experimental data are shown in Figure S6. Essentially, no changes are observed in the position of edge of the XANES spectra along the whole reaction (Figure 6a), but only a slight increase of the signal around 24395 eV is detected. The particle size distribution determined by analysing the SAXS data (Figure 6b) remain unchanged. In the EXAFS spectra, a slight shift of the Pd-X contribution towards longer distances is observed (from ca. 1.40 to 1.50 Å, not phase corrected), as well as a tiny decrease in the peak intensity. The fit of the EXAFS data (Table S3) confirms that R_{Pd-X} moves from ca. 2.04 ± 0.05 Å, typical for R_{Pd-O} in $Pd(OAc)_2$, to ca. 2.08 ±0.05 Å. This change is compatible with a reconstruction of the local environment around the Pd^{2+} cations. Only traces of acetic acid were detected by MS, at a temperature of 180 °C.

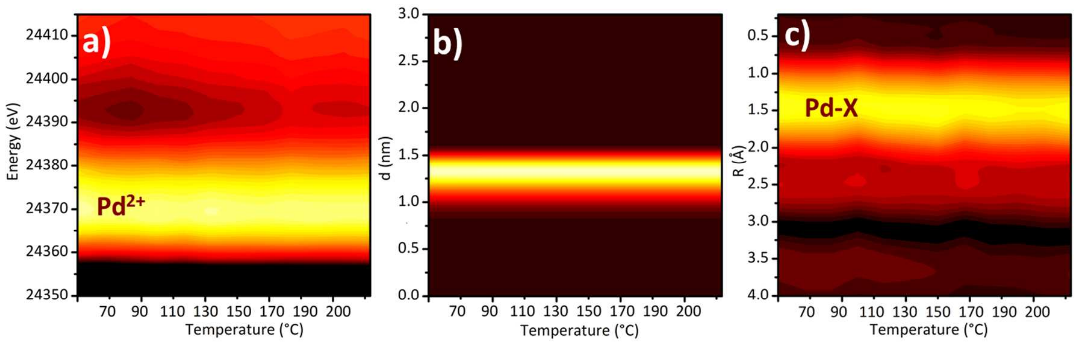

Figure 6. 2D maps showing the evolution of the XANES spectra (part a), of the particle size distribution as determined by the analysis of the SAXS data (part b), and of the amplitude of the phase-uncorrected FT of the EXAFS spectra (part c) as a function of the reaction temperature, for the $Pd(OAc)_2$/P4VP reacting with molecular oxygen. The intensity increases from black to yellow. The labels refer to the main assignments.

3.2.2 Catalytic performances of the $Pd(OAc)_2$/P4VP pre-oxidized in molecular oxygen

Also the $Pd(OAc)_2$/P4VP catalyst pre-oxidized in molecular oxygen efficiently catalyses the aerobic oxidation of 2-propanol to acetone. The reaction starts around 80-90 °C, as determined by DRIFT spectroscopy (appearance of the absorption band around 1730 cm^{-1} due to acetone, Figure S6) and by MS measurements (Figure 7d and d'). The maximum conversion is achieved around 150 °C, i.e. at a slightly lower temperature than for the pre-reduced catalyst. Figure 7 displays the results of the synchronous XAS/SAXS/MS experiment during the aerobic oxidation of 2-propanol on the pre-oxidized $Pd(OAc)_2$/P4VP catalyst, while the raw experimental spectra are reported in Figure S8. During the whole reaction, no changes are detected by any technique, indicating that highly dispersed Pd^{2+} cations stabilized by the pyridyl groups in P4VP are the active sites in the reaction. Noticeably, the catalyst is highly stable also at 180 °C, in contrast to what was observed after pre-reduction.

It is difficult to determine whether the Pd^{2+} cations are isolated or aggregated in small Pd-oxo clusters. In this respect, it is worth noticing that atomically dispersed Pd^{2+} species in a ultra-diluted mesoporous 0.03 wt% Pd/Al_2O_3 catalyst showed an exceptional activity in the selective oxidation of alcohols.[34] Pd_1O_4 single□sites anchored on the internal surface of micropores of a microporous silicate exhibit high selectivity and activity in the partial oxidation of CH_4 to CH_3OH with H_2O_2.[78] On the other hand, a trinuclear $[(LPd^{II})_3(\mu^3\text{-}O)_2]^{2+}$ intermediate compound has been recently identified during O_2 activation by Pd complexes and shown to be chemically and kinetically competent intermediate in catalytic alcohol oxidation reactions.[79] Our experimental data are compatible with the presence of both atomically dispersed Pd^{2+} species and ultra-small Pd-oxo clusters.

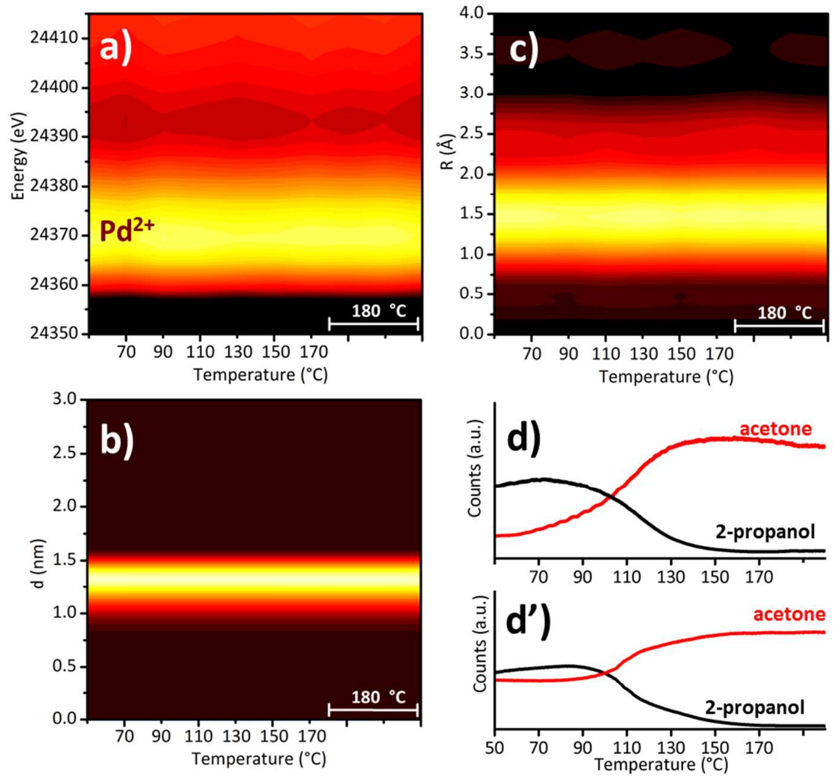

Figure 7. 2D maps showing the evolution of the XANES spectra (part a), of the particle size distribution as determined by the analysis of the SAXS data (part b), and of the amplitude of the phase-uncorrected FT of the EXAFS spectra (part c) as a function of the reaction temperature, for the $Pd(OAc)_2$/P4VP pre-oxidized in molecular oxygen during the aerobic oxidation of 2-propanol. The intensity increases from black to yellow. Parts d and d' shows the conversion of 2-propanol (m/Z = 45) into acetone (m/Z = 43) as detected by online MS and by an independent catalytic test performed with the CATLAB micro-reactor, respectively.

3.3 Aerobic oxidation of 2-propanol over un-treated $Pd(OAc)_2$/P4VP

As a final step, we investigated the behaviour of the un-treated $Pd(OAc)_2$/P4VP catalyst in the oxidation of 2-propanol to acetone in the same reaction conditions adopted for the pre-reduced and pre-oxidized catalysts. Three successive reaction cycles were performed to test the catalyst stability. Figure 8 summarizes the main results. During the first cycle, 2-propanol starts to be oxidized to acetone only at ca. 160 – 170 °C, as determined by DRIFT spectroscopy (Figure 8a1) and synchronous MS (Figure 8b1), as well as by the independent catalytic test performed with the CATLAB micro-reactor (Figure 8c1). The reason is that the Pd^{2+} cations need to loose (at least partially) the acetate ligands. Indeed, the XANES spectra (Figure 8d1) slightly change upon increasing the temperature, in the same way as was observed during the treatment in only O_2 (Figure 6a). This indicates that the active phase is not $Pd(OAc)_2$, but the cationic Pd^{2+} species in a different environment.

In the successive cycles (second, Figure 8a2 – Figure 8d2, and third Figure 8a3 – Figure 8d3) the oxidation of 2-propanol to acetone starts around 100 – 110 °C, reaching the maximum conversion at ca. 150 °C. The XANES spectra (as well as the EXAFS spectra and the SAXS patterns) do not change anymore (Figure 8d2 – Figure 8d3). The catalyst is highly stable even at 180 °C.

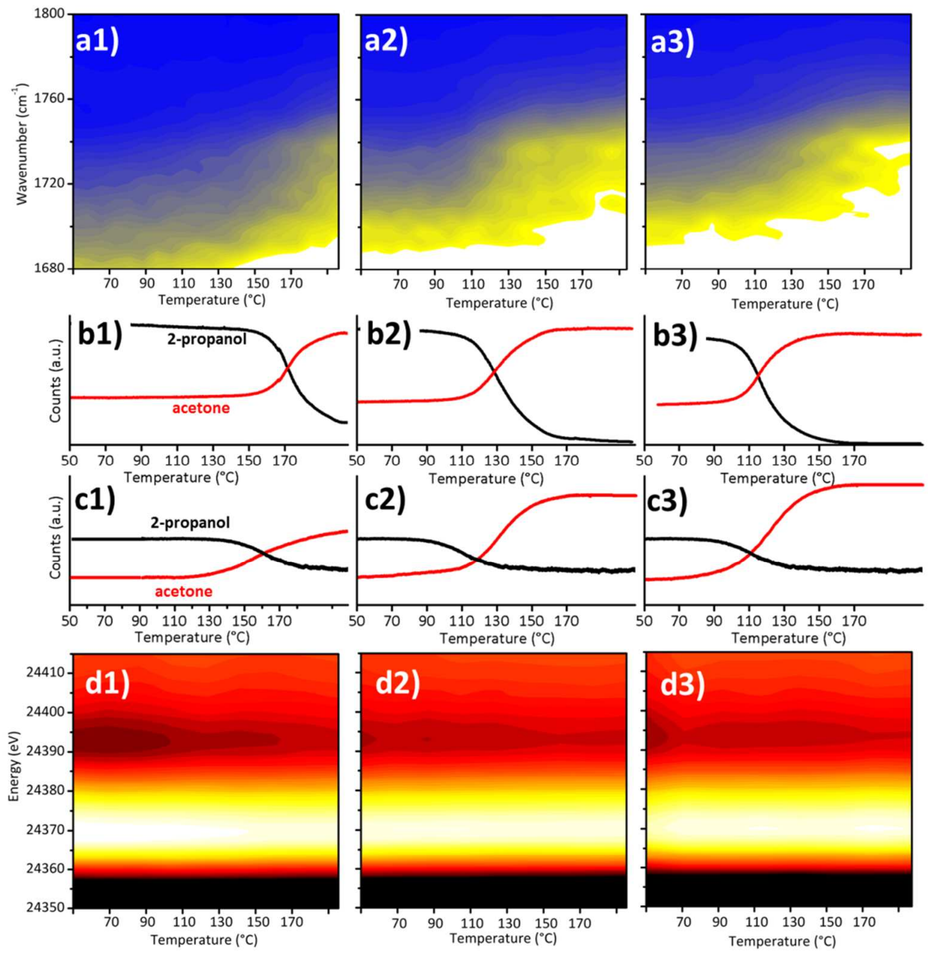

Figure 8. Part a1) 2D map showing the evolution of the DRIFT spectra as a function of the reaction temperature, for the un-treated $Pd(OAc)_2$/P4VP catalyst during the aerobic oxidation of 2-propanol. The intensity increases from black to yellow. Parts b1) and c1) conversion of 2-propanol (*m/Z* = 45) into acetone (*m/Z* = 43) as detected by online MS and by an independent catalytic test performed with the CATLAB micro-reactor, respectively. Part d1) 2D map showing the evolution of the XANES spectra as a function of the reaction temperature, for the un-treated $Pd(OAc)_2$/P4VP during the aerobic oxidation of 2-propanol. The intensity increases from black to yellow. Parts a2) – d2) and a3) – d3) are the same for the second and third reaction cycles, respectively.

4. Conclusions

We have investigated the behaviour of a heterogeneous $Pd(OAc)_2$/P4VP catalyst that mimics the most famous and widely employed homogeneous $Pd(OAc)_2$/pyridine system, during the gas-phase aerobic oxidation of 2-propanol to acetone. The combined use of synchronous SAXS/XAS/MS, coupled with *operando* DRIFT spectroscopy and HR-TEM, reveals to be a strategic approach to unravel simultaneously the oxidation state and the aggregation of the Pd phase under reaction conditions, at the same time monitoring the catalytic performances. In particular, we have demonstrated the following:

1) $Pd(OAc)_2$ in P4VP is reduced by 2-propanol in the 110 – 170 °C temperature range, leading to highly dispersed Pd^0 nano-particles with a very homogeneous particle size, which are stabilized by the pyridyl ligands in P4VP, similarly to what previously found in the presence of H_2.[47,48]
2) These Pd^0 nano-particles are rapidly and almost completely oxidized in the presence of the 2-propanol-O_2 reaction mixture (at least when the O_2 concentration is 15 vol%), already at low temperature (50 °C). The oxidized PdO nano-particles efficiently oxidize 2-propanol in acetone starting from ca. 110 °C. No variation in both particle size and Pd oxidation state are registered until 170 °C. This demonstrates the fundamental role of surface PdO in the adopted reaction conditions, in good agreement with the recent literature on the Pd catalysed selective oxidation of alcohols.[30-35] At temperature higher than 170 °C the PdO nano-particles are suddenly reduced and aggregate to form larger particles, with a consequent slight decrease of the catalytic activity.
3) In the presence of only O_2 at ca. 180 – 200 °C $Pd(OAc)_2$ in P4VP loses a fraction of the acetate ligands, with the consequent formation of isolated Pd^{2+} cations or ultra-small Pd-oxo clusters or both, stabilized by the pyridyl ligands in P4VP.
4) These Pd^{2+} cationic species catalyse the oxidation of 2-propanol to acetone starting from ca. 100 °C (i.e. at a temperature slightly lower than the pre-reduced catalyst). The catalyst remains in the reaction mixture stable also when reaching 180 °C.
5) The un-treated catalyst does not work in the reaction until a fraction of the acetate ligands are removed, which occurs around 170 – 180 °C. At that point, the catalyst behaves as the pre-oxidized one: it converts 2-propanol to acetone starting from ca. 100 °C, without any change in the Pd oxidation state and aggregation, even at 180 °C and for several reaction cycles, proving that the reaction occurs at a single site even though a heterogeneous system is used.

Observations 3)-5) clearly demonstrate that highly isolated Pd^{2+} cationic species, either atomically dispersed or in the form of ultra-small Pd^{2+}-oxo clusters, are efficient and very stable active sites for the gas-phase aerobic oxidation of 2-propanol. These results are in very good agreement with recent findings that both atomically dispersed Pd^{2+} species in a heterogeneous ultra-diluted catalyst[34] and multi-nuclear Pd-oxo homogeneous complexes[39,79] are active species implicated in the Pd-catalyzed aerobic oxidation reactions. It is important to remark, however, that our experiments have been conducted in excess of oxygen, and that a different outcome could have been obtained in other experimental conditions. Noticeably, the behaviour of the $Pd(OAc)_2$/P4VP catalyst under reaction conditions is influenced by the nature of the support. On one hand, the presence of the pyridyl functional groups is fundamental to stabilize the cationic Pd^{2+} species, exactly as for the ligand-modulated homogeneous Pd^{2+} complexes. On the other hand, the porous structure of the P4VP polymer efficiently confine the active Pd^{2+} species in the presence of the reagents. We can state that our $Pd(OAc)_2$/P4VP catalyst is situated at the confluence between its homogeneous and heterogeneous analogues.

Supporting Information.

Raw experimental DRIFTS, SAXS and XAS data; details on the EXAFS data analysis; results of the EXAFS fit.

Acknowledgements

ALB and CL acknowledge the Russian Ministry of Education and Science for financial support (Project RFMEFI58417X0029, Agreement 14.584.21.0029) for funding the research in Rostov-on-Don.

References

(1) Mallat, T.; Baiker, A., Oxidation Of Alcohols With Molecular Oxygen On Solid Catalysts, *Chem. Rev.* **2004**, *104*, 3037-3058.

(2) Lee, A. F., *Mechanistic Studies Of Alcohol Selective Oxidation*, In: Heterogeneous Catalysts For Clean Technology. Spectroscopy, Design, And Monitoring; Wilson, K.; Lee, A. F., Ed.; Wiley-VCH Verlag & Co. Kgaa,: Weinheim, Germany, **2014**, P. 11-38.

(3) Durndell, L. J.; Lee, A. F.; Bailie, D. S.; Muldoon, M. J., *Selective Palladium-Catalysed Aerobic Oxidation Of Alcohols*, In: Transition Metal Catalysis In Aerobic Alcohol Oxidation; Cardona, F.; Parmeggiani, C., Ed.; The Royal Society Of Chemistry: Cambridge, UK, **2015**, P. 92-132.

(4) Muhler, M., *Oxidative Dehydrogenation Of Alcohols To Aldehydes, Ketones And Carboxylic Acids*, In: Handbook Of Heterogeneous Catalysis; Ertl, G.; Knozinger, H.; Weitkamp, J., Ed.; VCH: Weinheim, **1997**; Vol. 5, P. 2274.

(5) Mallat, T.; Baiker, A., *Oxidation Of Alcohols With Molecular Oxygen*, In: Handbook Of Heterogeneous Catalysis; Ertl, G.; Knozinger, H.; Weitkamp, J., Ed.; Wiley-VCH Verlag Gmbh & Co. Kgaa, **2008**, P. 3521–3538.

(6) Stahl, S. S., Palladium-Catalyzed Oxidation Of Organic Chemicals With O2, *Science* **2005**, *309*, 1824.

(7) Cavani, F.; Teles, J. H., Sustainability In Catalytic Oxidation: An Alternative Approach Or A Structural Evolution?, *Chemsuschem* **2009**, *2*, 508–534.

(8) Montemore, M. M.; Van Spronsen, M. A.; Madix, R. J.; Friend, C. M., O2 Activation By Metal Surfaces: Implications For Bonding And Reactivity On Heterogeneous Catalysts, *Chem. Rev.* **2018**, *118*, 2816-2862.

(9) Centi, G.; Cavani, F.; Trifirò, F., *Selective Oxidation By Heterogeneous Catalysis*; Twigg, M. V.; Spencer, M. S., Ed.; Springer Science+Business Media, LLC: New York, **2001**.

(10) Beale, A. M.; Jacques, S. D. M.; Weckhuysen, B. M., Chemical Imaging Of Catalytic Solids With Synchrotron Radiation, *Chem. Soc. Rev.* **2010**, *39*, 4656-4672.

(11) Grunwaldt, J.-D.; Schroer, C. G., Hard And Soft X-Ray Microscopy And Tomography In Catalysis: Bridging The Different Time And Length Scales, *Chem. Soc. Rev.* **2010**, *39*, 4741-4753.

(12) Jung, U.; Elsen, A.; Li, Y.; Smith, J. G.; Small, M. W.; Stach, E. A.; Frenkel, A. I.; Nuzzo, R. G., Comparative In Operando Studies In Heterogeneous Catalysis: Atomic And Electronic Structural Features In The Hydrogenation Of Ethylene Over Supported Pd And Pt Catalysts, *ACS Catal.* **2015**, *5*, 1539-1551.

(13) Gai, P. L.; Sharma, R.; Ross, F. M., Environmental (S)TEM Studies Of Gas–Liquid–Solid Interactions Under Reaction Conditions, *MRS Bulletin* **2011**, *33*, 107-114.

(14) Li, Y.; Zakharov, D.; Zhao, S.; Tappero, R.; Jung, U.; Elsen, A.; Baumann, P.; Nuzzo, R. G.; Stach, E. A.; Frenkel, A. I., Complex Structural Dynamics Of Nanocatalysts Revealed In Operando Conditions By Correlated Imaging And Spectroscopy Probes, *Nature Comm.* **2015**, *6*.

(15) Ferri, D.; Baiker, A., Advances In Infrared Spectroscopy Of Catalytic Solid–Liquid Interfaces: The Case Of Selective Alcohol Oxidation, *Top. Catal.* **2009**, *52*, 1323-1333.

(16) Grunwaldt, J. D.; Caravati, M.; Baiker, A., Oxidic Or Metallic Palladium: Which Is The Active Phase In Pd-Catalyzed Aerobic Alcohol Oxidation?, *J. Phys. Chem. B* **2006**, *110*, 25586-25589.

(17) Steinhoff, B. A.; Guzei, I. A.; Stahl, S. S., Mechanistic Characterization Of Aerobic Alcohol Oxidation Catalyzed By Pd(Oac)<Inf>2</Inf>/Pyridine Including Identification Of The Catalyst Resting State And The Origin Of Nonlinear [Catalyst] Dependence, *J. Am. Chem. Soc.* **2004**, *126*, 11268-11278.

(18) Williams, R. M.; Medlin, J. W., Benzyl Alcohol Oxidation On Pd(111): Aromatic Binding Effects On Alcohol Reactivity, *Langmuir* **2014**, *30*, 4642-4653.

(19) Ferri, D.; Mondelli, C.; Krumeich, F.; Baiker, A., Discrimination Of Active Palladium Sites In Catalytic Liquid-Phase Oxidation Of Benzyl Alcohol, *J. Phys. Chem. B* **2006**, *110*, 22982-22986.
(20) Hayashi, M.; Yamada, K.; Nakayama, S.-Z., Catalytic Hydrogen-Transfer Reactions Of Benzylic And Allylic Alcohols With Palladium Compounds In The Presence Of Vinyl Acetate Or Under An Ethylene Atmosphere, *J. Chem. Soc. Perkin. Trans. 1* **2000** 1501-1503.
(21) Keresszegi, C.; Mallat, T.; Baiker, A., Selective Transfer Dehydrogenation Of Aromatic Alcohols On Supported Palladium, *New J. Chem,* **2001**, *25*, 1163-1167.
(22) Grunwaldt, J.-D.; Keresszegi, C.; Mallat, T.; Baiker, A., In Situ EXAFS Study Of Pd/Al2O3 During Aerobic Oxidation Of Cinnamyl Alcohol In An Organic Solvent, *J. Catal.* **2003**, *213*, 291-295.
(23) Keresszegi, C.; Grunwaldt, J. D.; Mallat, T.; Baiker, A., In Situ EXAFS Study On The Oxidation State Of Pd/Al2O3 And Bi-Pd/Al2O3 During The Liquid-Phase Oxidation Of 1-Phenylethanol, *J. Catal.* **2004**, *222*, 268-280.
(24) Keresszegi, C.; Ferri, D.; Mallat, T.; Baiker, A., On The Role Of CO Formation During The Aerobic Oxidation Of Alcohols On Pd/Al2O3: An In Situ Attenuated Total Reflection Infrared Study, *J. Catal.* **2005**, *234*, 64-75.
(25) Mondelli, C.; Ferri, D.; Grunwaldt, J.-D.; Krumeich, F.; Mangold, S.; Psaro, R.; Baiker, A., Combined Liquid-Phase ATR-IR And XAS Study Of The Bi-Promotion In The Aerobic Oxidation Of Benzyl Alcohol Over Pd/Al2O3, *J. Catal.* **2007**, *252*, 77-87.
(26) Lee, A. F.; Ellis, C. V.; Naughton, J. N.; Newton, M. A.; Parlett, C. M. A.; Wilson, K., Reaction-Driven Surface Restructuring And Selectivity Control In Allylic Alcohol Catalytic Aerobic Oxidation Over Pd, *J. Am. Chem. Soc.* **2011**, *133*, 5724-5727.
(27) Gaskell, C. V.; Parlett, C. M. A.; Newton, M. A.; Wilson, K.; Lee, A. F., Redox-Controlled Crotyl Alcohol Selective Oxidation: In Situ Oxidation And Reduction Dynamics Of Catalytic Pd Nanoparticles Via Synchronous XANES/MS, *ACS Catal.* **2012**, *2*, 2242-2246.
(28) Dirkx, J. M. H.; Van Der Baan, H. S., The Oxidation Of Glucose With Platinum On Carbon As Catalyst, *J. Catal.* **1981**, *67*, 1-13.
(29) Gangwal, V. R.; Van Der Schaaf, J.; Kuster, B. F. M.; Schouten, J. C., Noble-Metal-Catalysed Aqueous Alcohol Oxidation: Reaction Start-Up And Catalyst Deactivation And Reactivation, *J. Catal.* **2005**, *232*, 432-443.
(30) Lee, A. F.; Wilson, K., Structure-Reactivity Correlations In The Selective Aerobic Oxidation Of Cinnamyl Alcohol: In Situ XAFS, *Green Chem.* **2004**, *6*, 37-42.
(31) Lee, A. F.; Hackett, S. F. J.; Hargreaves, J. S. J.; Wilson, K., On The Active Site In Heterogeneous Palladium Selox Catalysts, *Green Chem.* **2006**, *8*, 549-555.
(32) Parlett, C. M. A.; Bruce, D. W.; Hondow, N. S.; Lee, A. F.; Wilson, K., Support-Enhanced Selective Aerobic Alcohol Oxidation Over Pd/Mesoporous Silicas, *ACS Catal.* **2011**, *1*, 636-640.
(33) Parlett, C. M. A.; Keshwalla, P.; Wainwright, S. G.; Bruce, D. W.; Hondow, N. S.; Wilson, K.; Lee, A. F., Hierarchically Ordered Nanoporous Pd/SBA-15 Catalyst For The Aerobic Selective Oxidation Of Sterically Challenging Allylic Alcohols, *ACS Catal.* **2013**, *3*, 2122-2129.
(34) Hackett, S. F. J.; Brydson, R. M.; Gass, M. H.; Harvey, I.; Newman, A. D.; Wilson, K.; Lee, A. F., High-Activity, Single-Site Mesoporous Pd/Al2O3 Catalysts For Selective Aerobic Oxidation Of Allylic Alcohols, *Angew. Chem.* **2007**, *119*, 8747-8750.
(35) Parlett, C. M. A.; Durndell, L. J.; Wilson, K.; Bruce, D. W.; Hondow, N. S.; Lee, A. F., Selective Oxidation Of Allylic Alcohols Over Highly Ordered Pd/Meso-Al2O3 Catalysts, *Catalysis Commun.* **2014**, *44*, 40-45.
(36) Stahl, S. S., Palladium Oxidase Catalysis: Selective Oxidation Of Organic Chemicals By Direct Dioxygen-Coupled Turnover, *Angew. Chem. Int. Ed.* **2004**, *43*, 3400-3420.

(37) Conley, N. R.; Labios, L. A.; Pearson, D. M.; Mccrory, C. C. L.; Waymouth, R. M., Aerobic Alcohol Oxidation With Cationic Palladium Complexes: Insights Into Catalyst Design And Decomposition, *Organometallics* **2007**, *26*, 5447-5453.

(38) Nielsen, R. J.; Goddard, W. A., Mechanism Of The Aerobic Oxidation Of Alcohols By Palladium Complexes Of N-Heterocyclic Carbenes, *J. Am. Chem. Soc.* **2006**, *128*, 9651-9660.

(39) Ingram, A. J.; Walker, K. L.; Zare, R. N.; Waymouth, R. M., Catalytic Role Of Multinuclear Palladium–Oxygen Intermediates In Aerobic Oxidation Followed By Hydrogen Peroxide Disproportionation, *J. Am. Chem. Soc.* **2015**, *137*, 13632-13646.

(40) Scheuermann, M. L.; Goldberg, K. I., Reactions Of Pd And Pt Complexes With Molecular Oxygen, *Chem. Eur. J.* **2014**, *20*, 14556-14568.

(41) Jaworski, J. N.; Mccann, S. D.; Guzei, I. A.; Stahl, S. S., Detection Of Palladium(I) In Aerobic Oxidation Catalysis, *Angew. Chem.-Int. Edit.* **2017**, *56*, 3605-3610.

(42) Steinhoff, B. A.; Fix, S. R.; Stahl, S. S., Mechanistic Study Of Alcohol Oxidation By The Pd(Oac)<Inf>2</Inf>/O<Inf>2</Inf>/DMSO Catalyst System And Implications For The Development Of Improved Aerobic Oxidation Catalysts, *J. Am. Chem. Soc.* **2002**, *124*, 766-767.

(43) Steinhoff, B. A.; Stahl, S. S., Mechanism Of Pd(Oac)<Inf>2</Inf>/DMSO-Catalyzed Aerobic Alcohol Oxidation: Mass-Transfer-Limitation Effects And Catalyst Decomposition Pathways, *J. Am. Chem. Soc.* **2006**, *128*, 4348-4355.

(44) Nishimura, T.; Onoue, T.; Ohe, K.; Uemura, S., Palladium(II)-Catalyzed Oxidation Of Alcohols To Aldehydes And Ketones By Molecular Oxygen, *J. Org. Chem.* **1999**, *64*, 6750-6755.

(45) Steinhoff, B. A.; Stahl, S. S., Ligand-Modulated Palladium Oxidation Catalysis: Mechanistic Insights Into Aerobic Alcohol Oxidation With The Pd(Oac)2/Pyridine Catalyst System, *Organic Lett.* **2002**, *4*, 4179-4181.

(46) Steinhoff, B. A.; King, A. E.; Stahl, S. S., Unexpected Roles Of Molecular Sieves In Palladium-Catalyzed Aerobic Alcohol Oxidation, *J. Org. Chem.* **2006**, *71*, 1861-1868.

(47) Groppo, E.; Liu, W.; Zavorotynska, O.; Agostini, G.; Spoto, G.; Bordiga, S.; Lamberti, C.; Zecchina, A., Sub-Nanometric Pd Particles Stabilized Inside Highly Cross-Linked Polymeric Supports, *Chem. Mater.* **2010**, *22*, 2297-2308.

(48) Groppo, E.; Agostini, G.; Borfecchia, E.; Lazzarini, A.; Liu, W.; Lamberti, C.; Giannici, F.; Portale, G.; Longo, A., The Pyridyl Functional Groups Guide The Formation Of Pd Nanoparticles Inside A Porous Poly(4-Vinyl-Pyridine), *Chemcatchem* **2015**, *7*, 2188-2195.

(49) Longo, A.; Lamberti, C.; Agostini, G.; Borfecchia, E.; Lazzarini, A.; Liu, W.; Giannici, F.; Portale, G.; Groppo, E., Pd Nanoparticles Formation Inside Porous Polymeric Scaffolds Followed By In Situ XANES/SAXS, *J. Phys.* **2016**, *712*.

(50) Lazzarini, A.; Groppo, E.; Agostini, G.; Borfecchia, E.; Giannici, F.; Portale, G.; Longo, A.; Pellegrini, R.; Lamberti, C., Formation And Growth Of Palladium Nanoparticles Inside Porous Poly(4-Vinyl-Pyridine) Monitored By Operando Techniques: The Role Of Different Reducing Agents, *Catal. Today* **2017**, *283*, 144-150.

(51) Note That The Pd Loading Was Selected In Order To Maximize The Amount Of Pd, At The Same Time Keeping The Pd Dispersion As High As Possible. 4 Wt% Corresponds To Half Of The Adsorption Capacity Of The P4VP Support.

(52) Nikitenko, S.; Beale, A. M.; Van Der Eerden, A. M. J.; Jacques, S. D. M.; Leynaud, O.; O'Brien, M. G.; Detollenaere, D.; Kaptein, R.; Weckhuysen, B. M.; W., B., Implementation Of A Combined SAXS/WAXS/QEXAFS Set-Up For Time-Resolved In Situ Experiments, *J. Synchrotron Rad.* **2008**, *15*, 632-640.

(53) Longo, A.; Portale, G.; Bras, W.; Giannici, F.; Ruggirello, A. M.; Turco Liveri, V., Structural Characterization Of Frozen N-Heptane Solutions Of Metal-Containing Reverse Micelles, *Langmuir* **2007**, *23*, 11482-11487.

(54) Martis, V.; Beale, A. M.; Detollenaere, D.; Banerjee, D.; Moroni, M.; Gosselin, F.; Bras, W., A High-Pressure And Controlled-Flow Gas System For Catalysis Research, *J. Synchrotron Rad.* **2014**, *21*, 462-463.

(55) Rehr, J. J.; Albers, R. C., Theoretical Approaches To X-Ray Absorption Fine Structure, *Rev. Mod. Phys.* **2000**, *72*, 621-654.

(56) Filipponi, A.; Di Cicco, A.; Natoli, C. R., X-Ray-Absorption Spectroscopy And N-Body Distribution Functions In Condensed Matter. I. Theory, *Phys. Rev. B* **1995**, *52*, 15122-15134.

(57) Hammersley, A., FIT2D: A Multi-Purpose Data Reduction, Analysis And Visualization Program, *J. Appl. Cryst.* **2016**, *49*, 646-652.

(58) ESRF Internal Report, ESRF98HA01T, FIT2D V9.129 Reference Manual V3.1 (1998).

(59) Tessier, D.; Rakai, A.; Bozonverduraz, F., Spectroscopic Study Of The Interaction Of Carbon-Monoxide With Cationic And Metallic Palladium In Palladium Alumina Catalysts, *J. Chem. Soc.-Faraday Trans.* **1992**, *88*, 741-749.

(60) Newton, M. A.; Brazier, J. B.; Barreiro, E. M.; Parry, S.; Emmerich, H.; Adrio, L. A.; Mulligan, C. J.; Hellgardt, K.; Hii, K. K., Operando XAFS Of Supported Pd Nanoparticles In Flowing Ethanol/Water Mixtures: Implications For Catalysis, *Green Chem.* **2016**, *18*, 406-411.

(61) Mccurdie, M. P.; Belfiore, L. A., Spectroscopic Analysis Of Transition-Metal Coordination Complexes Based On Poly(4-Vinylpyridine) And Dichlorotricarbonylruthenium(II), *Polymer* **1999**, *40*, 2889-2902.

(62) Wu, K. H.; Wang, Y. R.; Hwu, W. H., FTIR And TGA Studies Of Poly(4-Vinylpyridine-Co-Divinylbenzene)-Cu(II) Complex, *Polym. Degrad. Stabil.* **2003**, *79*, 195-200.

(63) Pardey, A. J.; Rojas, A. D.; Yanez, J. E.; Betancourt, P.; Scott, C.; Chinea, C.; Urbina, C.; Moronta, D.; Longo, C., Spectroscopic Characterization Of Coordination Complexes Based On Dichlorocopper(II) And Poly(4-Vinylpyridine): Application In Catalysis, *Polyhedron* **2005**, *24*, 511-519.

(64) Belfiore, L. A.; Mccurdie, M. P.; Ueda, E., Polymeric Coordination-Complexes Based On Cobalt, Nickel, And Ruthenium That Exhibit Synergistic Thermal-Properties, *Macromolecules* **1993**, *26*, 6908-6917.

(65) Belfiore, L. A.; Pires, A. T. N.; Wang, Y. H.; Graham, H.; Ueda, E., Transition-Metal Coordination In Polymer Blends And Model Systems, *Macromolecules* **1992**, *25*, 1411-1419.

(66) Groppo, E.; Uddin, M. J.; Bordiga, S.; Zecchina, A.; Lamberti, C., Structure And Redox Activity Of Copper Sites Isolated In A Nanoporous P4VP Polymeric Matrix, *Angew. Chem.-Int. Edit.* **2008**, *47*, 9269-9273.

(67) Groppo, E.; Agostini, G.; Borfecchia, E.; Wei, L.; Giannici, F.; Portale, G.; Longo, A.; Lamberti, C., Formation And Growth Of Pd Nanoparticles Inside A Highly Cross-Linked Polystyrene Support: Role Of The Reducing Agent, *J. Phys. Chem. C* **2014**, *118*, 8406-8415.

(68) Frenkel, A. I., Solving The Structure Of Nanoparticles By Multiple-Scattering EXAFS Analysis, *J. Synchrot. Radiat.* **1999**, *6*, 293-295.

(69) Frenkel, A. I.; Hills, C. W.; Nuzzo, R. G., A View From The Inside: Complexity In The Atomic Scale Ordering Of Supported Metal Nanoparticles, *J. Phys. Chem. B* **2001**, *105*, 12689-12703.

(70) Frenkel, A., Solving The 3D Structure Of Metal Nanoparticles, *Z. Kristall.* **2007**, *222*, 605-611.

(71) Witkowska, A.; Di Cicco, A.; Principi, E., Local Ordering Of Nanostructured Pt Probed By Multiple-Scattering XAFS, *Phys. Rev. B* **2007**, *76*.

(72) Agostini, G.; Pellegrini, R.; Leofanti, G.; Bertinetti, L.; Bertarione, S.; Groppo, E.; Zecchina, A.; Lamberti, C., Determination Of The Particle Size, Available Surface Area, And Nature Of Exposed Sites For Silica-Alumina-Supported Pd Nanoparticles: A Multitechnical Approach, *J. Phys. Chem. C* **2009**, *113*, 10485-10492.

(73) Agostini, G.; Piovano, A.; Bertinetti, L.; Pellegrini, R.; Leofanti, G.; Groppo, E.; Lamberti, C., Effect Of Different Face Centered Cubic Nanoparticle Distributions On Particle Size And Surface Area Determination: A Theoretical Study, *J. Phys. Chem. C* **2014**, *118*, 4085-4094.

(74) Sun, Y.; Frenkel, A. I.; Isseroff, R.; Shonbrun, C.; Forman, M.; Shin, K. W.; Koga, T.; White, H.; Zhang, L. H.; Zhu, Y. M.; Rafailovich, M. H.; Sokolov, J. C., Characterization Of Palladium Nanoparticles By Using X-Ray Reflectivity, EXAFS, And Electron Microscopy, *Langmuir* **2006**, *22*, 807-816.

(75) Lee, A. F.; Ellis, P. J.; Fairlamb, I. J. S.; Wilson, K., Surface Catalysed Suzuki-Miyaura Cross-Coupling By Pd Nanoparticles: An Operando XAS Study, *Dalton Trans.* **2010**, *39*, 10473-10482.

(76) Mouat, A. R.; Whitford, C. L.; Chen, B.-R.; Liu, S.; Perras, F. A.; Pruski, M.; Bedzyk, M. J.; Delferro, M.; Stair, P. C.; Marks, T. J., Synthesis Of Supported Pd0 Nanoparticles From A Single-Site Pd2+ Surface Complex By Alkene Reduction, *Chem. Mat.* **2018**, *30*, 1032-1044.

(77) It Is Worth Noticing That The Apparent Discrepancy Of The <Dsaxs> And <Dtem> Values Can Be Explained By Considering That The SAXS Signal Is Weighted For R6 (See Eq. 1), Hence Bigger Particles Contribute To The SAXS Signal Much More Than The Smaller Ones. On The Other Hand, The Particle Size Distribution Determined By HR-TEM Relies Only On The Small Particles

(78) Huang, W.; Zhang, S.; Tang, Y.; Li, Y.; Nguyen, L.; Li, Y.; Shan, J.; Xiao, D.; Gagne, R.; Frenkel, A. I.; Tao, F. F., Low-Temperature Transformation Of Methane To Methanol On Pd<Inf>1</Inf>O<Inf>4</Inf>Single Sites Anchored On The Internal Surface Of Microporous Silicate, *Angew. Chem.-Int. Edit.* **2016**, *55*, 13441-13445.

(79) Ingram, A. J.; Solis-Ibarra, D.; Zare, R. N.; Waymouth, R. M., Trinuclear Pd3O2 Intermediate In Aerobic Oxidation Catalysis, *Angew. Chem. Int. Ed.* **2014**, *53*, 5648-5652.

Table of Contents